Chemical Physics 440 (2014) 69–79

Contents lists available at ScienceDirect

Chemical Physics

journal homepage: www.elsevier.com/locate/chemphys

Protonation/deprotonation process of Emodin in aqueous solution and pK_a determination: UV/Visible spectrophotometric titration and quantum/molecular mechanics calculations

Antonio R. da Cunha, Evandro L. Duarte, M. Teresa Lamy, Kaline Coutinho *

Instituto de Física, Universidade de São Paulo, SP, Brazil

ARTICLE INFO

Article history:
Received 13 February 2014
In final form 11 June 2014
Available online 24 June 2014

Keywords:
Protonation/deprotonation process
Acidity constant
Deprotonation free energy
Theoretical calculation
Experimental measurement
UV/Visible spectrophotometric titration curves

ABSTRACT

We combined theoretical and experimental studies to elucidate the important deprotonation process of Emodin in water. We used the UV/Visible spectrophotometric titration curves to obtain its pK_a values, $pK_{a1} = 8.0 \pm 0.1$ and $pK_{a2} = 10.9 \pm 0.2$. Additionally, we obtained the pK_a values of Emodin in the water–methanol mixture (1:3v/v). We give a new interpretation of the experimental data, obtaining apparent $pK_{a1} = 6.2 \pm 0.1$, $pK_{a2} = 8.3 \pm 0.1$ and $pK_{a3} > 12.7$.

Performing quantum mechanics calculations for all possible deprotonation sites and tautomeric isomers of Emodin in vacuum and in water, we identified the sites of the first and second deprotonation. We calculated the standard deprotonation free energy of Emodin in water and the pK_{a1}, using an explicit model of the solvent, with Free Energy Perturbation theory in Monte Carlo simulations obtaining, $\Delta G_{aq} = 12.1 \pm 1.4$ kcal/mol and $pK_{a1} = 8.7 \pm 0.9$. With the polarizable continuum model for the solvent, we obtained $\Delta G_{aq} = 11.6 \pm 1.0$ kcal/mol and $pK_{a1} = 8.3 \pm 0.7$. Both solvent models gave theoretical results in very good agreement with the experimental values.

1. Introduction

Emodin (1,3,8-trihydroxy-6-methyl-9,10-anthraquinone, Fig. 1) is one of the most abundant anthraquinone derivatives found in nature [1]. It is the active principle of herbal medicines deriving from Polygonaceae, Rhamnaceae and Cassieae [2]. This anthraquinone is known to have biological activity, such as anti-bacterial [3–5], antiviral [6,7], anti-inflammatory [8,9], anti-cancer activities [10–12] and virucidal agent [2].

The UV/Visible spectrum of the Emodin has been used to study its interaction with the biological environment, like DNA [13,14] and human serum albumin (HSA) [15], and also as a spectrophotometric reagent for detection of various metal ions [16]. Emodin is a yellow amorphous solid, insoluble in water at acidic *pH*, but red and soluble in water at alkaline *pH*. In acidic aqueous solution and in common organic solvents, there is a broad UV/Visible absorption band between 350 and 500 nm in the Emodin spectrum with a λ_{max} around 440 nm that is responsible for the yellow color of these solutions. In alkaline solutions, this broad band is red shifted to 450–600 nm with a λ_{max} varying between 520 and 555 nm depending on solvent and yielding a red color to these solutions. The UV/Visible absorption spectra and the first band λ_{max} of Emodin in several solvents in acidic and alkaline *pH* are presented in the Supplementary Material. It is known that this noticeable change in color of Emodin in solution with different *pH* is due to a deprotonation process [16]. The neutral form of the Emodin (EMH) is yellow and the anionic/deprotonated form (EM^-) is red. Based on the potentiometric titration of the Emodin in a methanol–water mixture, Pal and Jana [16] established the one-proton dissociation equilibrium in the range *pH* 2–10 and determined an apparent pK_{a1} of 7.2 in this mixture. They also suggested a stepwise dissociation of three protons: first in position 3 (3-oxido-6-methyl-1,8-dihydroxy-9,10-anthraquinone), second in position 8 (3,8-oxido-6-methyl-1-hydroxy-9,10-anthraquinone) and third in position 1 (1,3,8-oxido-6-methyl-9,10-anthraquinone). An experimental and theoretical investigation of the electronic transitions of Emodin and its conjugated base with deprotonation at position 3 in ethanol has been published [17]. They used synchrotron linear dichroism spectroscopy and quantum mechanics calculations with Density Functional Theory (TD-B3LYP/6-31+G(d,p)) to characterize the absorption spectrum of Emodin. In their calculation, the solvent was included using the polarizable continuum model (PCM) and one additional explicit solvent molecule hydrogen bonded to the deprotonated oxygen of Emodin.

* Corresponding author. Tel.: +55 1130916745.
E-mail addresses: antcunha@if.usp.br (A.R. da Cunha), elduarte@if.usp.br (E.L. Duarte), mtlamy@if.usp.br (M.T. Lamy), kaline@if.usp.br (K. Coutinho).

http://dx.doi.org/10.1016/j.chemphys.2014.06.009
0301-0104/

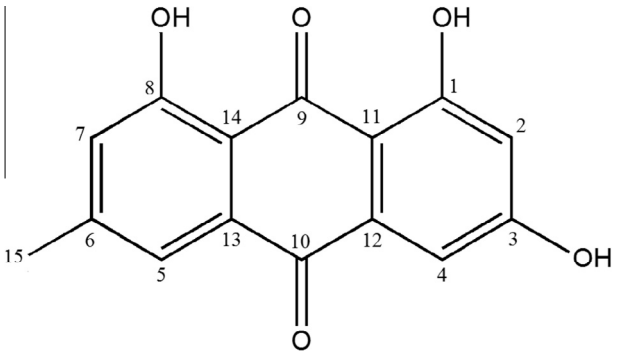

Fig. 1. Chemical structure and atomic numbering of Emodin in its neutral form (EMH).

The protonation/deprotonation process of a pharmacophore is a topic of large interest in physics, chemistry and pharmaceutical industry, because it can change the pharmacological activity of a compound [18,19]. Frequently, a well-defined acidity constant (pK_a) describes the chemical reactivity of molecules [20]. Hence, the determination of the value of the pK_a has been the object of many experimental and theoretical studies. The experimental methods commonly used for the determination of the pK_a are: dissolution rate method [21], ionophoretic techniques [22], isotachophoresis [23], conductivity [24], potentiometric titration [25], nuclear magnetic resonance spectroscopy [26], UV/Visible spectrophotometric titration [27], thermodynamics [28], Z-scan technique [29] and capillary electrophoresis [30]. On the other hand, the theoretical works have utilized computer simulations with explicit solvent models and Free Energy Perturbation [31–34], Poisson–Boltzmann equation with continuum solvent models [35,36], quantum mechanics calculation associated with continuum solvent models [37–42] and cluster based quantum mechanics calculation [43].

The protonation/deprotonation processes of Emodin in organic solutions were experimentally analyzed, and acidity constants of Emodin were determined in water–methanol [16], water–ethanol [17], water–acetonitrile and acetonitrile [30]. However, to our knowledge, experimental and theoretical studies of the Emodin in aqueous solution have never been reported. This is a non-trivial task, due to the low solubility of the Emodin in acidic aqueous solution [16].

In the present work, we study the protonation/deprotonation process of Emodin in aqueous solution, using experimental and theoretical techniques. With the UV/Visible spectrophotometric titration technique, we determined the pK_a of Emodin in water. The solubility difficulty was minimized by titrating the Emodin in aqueous solution from alkaline to acidic pH (from 13.8 to 2.0), and measuring the UV/Visible absorption spectrum immediately after strongly vortexing the sample.

Additionally to the experimental assay, we performed a theoretical study to identify the position of the first deprotonation of Emodin in aqueous solution. The theoretical approach was based in thermodynamic cycles obtained from two different equilibrium reactions, $XH \Longleftrightarrow X^- + H^+$ and $XH + H_2O \Longleftrightarrow X^- + H_3O^+$, where the XH is the molecule of interest and the reactions were investigated in gas phase and in aqueous solution. These thermodynamic cycles were previously used [39,40,44,45] to calculate the deprotonation free energy of the XH in aqueous solution (ΔG_{aq}), and additionally the pK_a. The values of the ΔG_{aq} were calculated using an expression, obtained from the thermodynamic cycle, that relates ΔG_{aq} with the free energy of deprotonation in gas phase (ΔG_g) and the relative free energies of solvation ($\Delta\Delta G_{solv}$) of the neutral and ionic species involved in the reactions ($\Delta G_{aq} = \Delta G_g + \Delta\Delta G_{solv}$).

The ΔG_g was computed by quantum mechanical calculations, using Density Functional Theory (DFT) and Møller–Plesset second order perturbation theory (MP2). All the possibilities of the first deprotonation form and the tautomeric isomers of the Emodin in gas phase and in aqueous solution were analyzed. We identified that the first deprotonation at position 3 and the second deprotonation at position 8 are the most favored situation. This result is in agreement with the Pal and Jana suggestion [16]. The solvation free energies of each Emodin species, ΔG_{solv}(EMH) and ΔG_{solv}(EM^-), were calculated using Monte Carlo (MC) simulations combined with Free Energy Perturbation theory (FEP) and the ΔG_{aq} values were obtained using the two thermodynamic cycles. Finally, the theoretical value for the pK_{a1} was obtained and it presents a very good agreement with the experimental data.

2. Experimental

2.1. Materials

Emodin ($C_{15}H_{10}O_5$, Fig. 1), Hydrochloric acid (HCl), Sodium hydroxide (NaOH) and Methanol (CH_3OH) were purchased from Sigma–Aldrich Co. (St. Louis, MO, USA) and used without further purification. Milli-Q water was used throughout.

2.2. Sample preparation

A 10 mM Emodin stock solution was prepared in ethanol-methanol mixture at 4:1 v/v. Aliquots of this stock solution were separated in glass vials, dried under a stream of N_2, and left under reduced pressure for a minimum of two hours, to remove traces of organic solvents. The Emodin film so formed was dissolved in water at two different concentrations, 0.1 and 0.025 mM, and in water–methanol mixture (1:3 v/v) at concentration of 0.025 mM. For each concentration, two different pH samples were prepared at room temperature: an alkaline at $pH \sim 13$, and an acidic at $pH \sim 2$, by the addition of NaOH and HCl, respectively. In water, at $pH \sim 2$ the Emodin aggregates, and precipitates after a minute, hence the sample had to be strongly vortexed before used.

2.3. UV/Visible spectrophotometric titration

Absorbance measurements were performed with a Varian Cary 50 UV/Visible Spectrophotometer, at room temperature. Samples were placed in quartz cuvettes with 10 mm optical pathway. Absorbance measurements of the Emodin solution samples were performed from alkaline to acidic pH values, by successive addition of small aliquots (around 5 μL) of the Emodin acidic solution (1:500 v/v of HCl). For the two studied concentrations, two independent samples were prepared for each pH and around 70 UV/Visible spectra were measured in the pH interval, from ~13 to 2. The samples were homogenized by strongly vortexing immediately before each measurement and its pH was measured with a Mettler Toledo pH-meter. Therefore, in the case of the water–methanol mixture the pH presented are the apparent pH values.

2.4. Determination of acidity constant

The deprotonation probability of a single site in a solute molecule is given by Eq. (1), algebraically equivalent to the Henderson–Hasselbalch (HH) equation, describing an increasing sigmoidal standard titration curves:

$$\xi = \frac{10^{(pH-pK_a)}}{(1+10^{(pH-pK_a)})} \quad (1)$$

Hence, the pK_a value of an isolated titratable site is equal to the pH at which the deprotonation probability of this site is 0.5 and the concentration of the deprotonated form ($[EM^-]$) is given by

$$[EM^-] = \frac{[EM]10^{(pH-pK_a)}}{\left(1+10^{(pH-pK_a)}\right)} \quad (2)$$

where $[EM] = [EMH] + [EM^-]$ is the total concentration of the solute as a sum of the neutral and anionic/deprotonated forms.

For n multiple decoupled deprotonation process, the probability of deprotonating each site i is then given by the HH titration curve

$$\xi_i = \frac{10^{(pH-pK_{ai})}}{(1+10^{(pH-pK_{ai})})} \quad \text{and} \quad [EM^{-i}] = \frac{[EM]10^{(pH-pK_{ai})}}{(1+10^{(pH-pK_{ai})})} \quad (3)$$

where $K_i = 10^{-pK_{ai}}$ is the deprotonation constant of site i, $[EM^{-i}]$ is the concentration of the ith deprotonated form, $[EM]$ is the total concentration of the solute as a sum of the neutral form and the deprotonated forms, and the total probability of the molecule deprotonation is just the sum of individual HH curves [46].

Using the UV/Visible spectrophotometric titration (UV/Visible ST) [47] and assuming that the n possible deprotonation forms of a chromophore solute are decoupled and non-interacting, the Bouguer–Lambert–Beer law can be written by a sum of individual absorbance:

$$A \equiv \log\left(\frac{I_0}{I}\right) = \varepsilon_0[EMH]l + \sum_{i=1}^{n}\varepsilon_i[EM^{-i}]l \quad (4)$$

where A is the measured absorbance, I_0 and I are the intensities of the light at a fixed wavelength before and after crossing the sample, respectively, ε_0 and ε_n are the molar extinction coefficient of the neutral and nth deprotonated form, respectively, and l is the optical pathlength. Therefore, Eqs. (3) and (4) yield the following generalized expression:

$$A = A_0 + \sum_{i=1}^{n} A_i \frac{10^{(pH-pK_{ai})}}{\left(1+10^{(pH-pK_{ai})}\right)} \quad (5)$$

where A is the total absorbance measured of the system at a given wavelength and A_0, A_i and pK_{ai} values are determined by the best fitting of the UV/Visible ST curve, over the range of pH values, in which A increases with an increasing pH. Note that, in a specific wavelength, if A decreases in a range of pH, then the term $pH–pK_{ai}$ of Eq. (5) should be inverted to $pK_{ai}–pH$ for describing a decreasing sigmoidal standard titration curve. Thus, the experimental values for the acidity constants pK_{ai} were obtained using the UV/Visible ST curves and the best fitting of the Eq. (5).

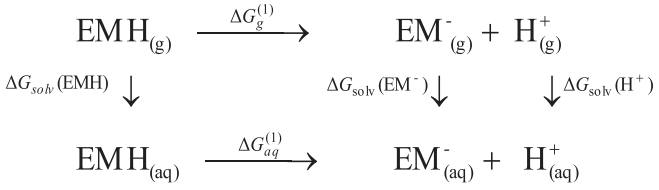

Scheme 1. The thermodynamic cycle 1 with the direct dissociation of the Emodin in the anionic specie (EM^-) and the proton (H^+) in gas phase and in aqueous solution.

3. Theoretical calculations

3.1. Thermodynamic cycles

The theoretical approach was based in two different thermodynamic cycles, shown in Schemes 1 and 2, to calculate the free energy of deprotonation in aqueous solution, ΔG_{aq}, and additionally the pK_a. Both thermodynamic cycles combine the deprotonation process of Emodin in gas phase and in aqueous solution. In the Scheme 1, there is a direct dissociation of the neutral form of Emodin (EMH) into the deprotoned/anionic form (EM^-) and the proton (H^+), and in the Scheme 2, there is a base-acid reaction between the Emodin and water molecules producing the same anionic species, EM^-, and the hydronium cation (H_3O^+). It was discussed and shown by several authors [39,40,44,45] that both thermodynamic cycles give the same value of pK_a although the free energies involved are different. The $\Delta G^{(1)}_{aq}$ is the deprotonation free energy obtained from the direct dissociation reaction (shown in Scheme 1) and $\Delta G^{(2)}_{aq}$ is obtained from the base-acid reaction with the water molecule (shown in Scheme 2). Then, in the theoretical approach the expression that relates the pK_a and the ΔG_{aq} depends on the deprotonation reaction, but in the experimental approach the reported ΔG_{aq} is always associated to the direct dissociation reaction, i.e. the $\Delta G^{(1)}_{aq}$.

The thermodynamic cycle 1 yields the following equation to calculate the $\Delta G^{(1)}_{aq}$ using the free energy of deprotonation in gas phase, $\Delta G^{(1)}_{g}$, and the relative free energy of solvation, $\Delta\Delta G^{(1)}_{solv}$, of the neutral and ionic species:

$$\Delta G^{(1)}_{aq} = \Delta G^{(1)}_{aq} + \Delta\Delta G^{(1)}_{solv}, \quad (6)$$

where

$$\Delta G^{(1)}_{g} = G_g(EM^-) + G_g(H^+) - G_g(EMH)$$

$$\Delta G^{(1)}_{g} = (G_g(EM^-) - G_g(EMH)) + G_g(H^+)$$

$$\Delta G^{(1)}_{g} = \Delta G_g(\text{Emodin}) + G_g(H^+) \quad (7)$$

$$\Delta\Delta G^{(1)}_{solv} = \Delta G_{solv}(EM^-) + \Delta G_{solv}(H^+) - \Delta G_{solv}(EMH)$$

$$\Delta\Delta G^{(1)}_{solv} = (\Delta G_{solv}(EM^-) - \Delta G_{solv}(EMH)) + \Delta G_{solv}(H^+)$$

$$\Delta\Delta G^{(1)}_{solv} = \Delta\Delta G_{solv}(\text{Emodin}) + \Delta G_{solv}(H^+) \quad (8)$$

$G_g(X)$ is the free energy of a specific specie X (X = EMH, EM^- and H^+) in gas phase and $\Delta G_{solv}(X)$ is the solvation free energy of the species X in aqueous solution. Thus, the pK_{a1} is obtained through the use of acidity constant definition, $K_{a1} = [EM^-][H^+]/[EMH]$, that leads to the thermodynamics equation:

$$pK_{a1} = \frac{\Delta G^{(1)}_{aq}}{RT\ln 10} \quad (9)$$

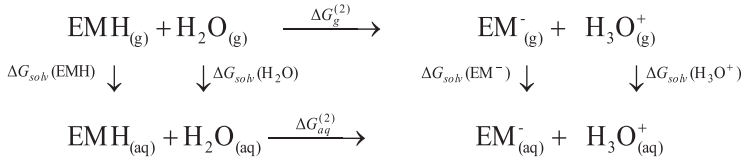

Scheme 2. The thermodynamic cycle 2 with the acid-base reaction between the Emodin and water in gas phase and in aqueous solution.

where R is the ideal gas constant. Then, $pK_{a1} = 0.733\ \Delta G^{(1)}_{aq}$ at 25 °C.

The thermodynamic cycle 2 yields the following equation to calculate the $\Delta G^{(2)}_{aq}$ that is equivalent to Eq. (6):

$$\Delta G^{(2)}_{aq} = \Delta G^{(2)}_{aq} + \Delta\Delta G^{(2)}_{solv}, \tag{10}$$

where

$$\Delta G^{(2)}_{g} = G_g(EM^-) + G_g(H_3O^+) - G_g(EMH) - G_g(H_2O)$$

$$\Delta G^{(2)}_{g} = (G_g(EM^-) - G_g(EMH)) + (G_g(H_3O^+) + G_g(H_2O))$$

$$\Delta G^{(2)}_{g} = \Delta G_g(\text{Emodin}) + \Delta G_g(\text{Water}) \tag{11}$$

$$\Delta\Delta G^{(2)}_{solv} = \Delta G_{solv}(EM^-) + \Delta G_{solv}(H_3O^+) - \Delta G_{solv}(EMH) - \Delta G_{solv}(H_2O)$$

$$\Delta\Delta G^{(2)}_{solv} = (\Delta G_{solv}(EM^-) - \Delta G_{solv}(EMH)) + (\Delta G_{solv}(H_3O^+) - \Delta G_{solv}(H_2O))$$

$$\Delta\Delta G^{(2)}_{solv} = \Delta\Delta G_{solv}(\text{Emodin}) + \Delta\Delta G_{solv}(\text{Water}) \tag{12}$$

Now the acidity constant is defined as $K_{a1} = [EM^-][H_3O^+]/[EMH]$ and the pK_{a1} is obtained through the relation:

$$pK_{a1} = \frac{\Delta G^{(2)}_{aq}}{RT\ln 10} - \log[H_2O] \tag{13}$$

where $[H_2O] = 55.50$ M is the water concentration at room thermodynamic condition of T and P. Then, $pK_{a1} = 0.733\ \Delta G^{(2)}_{aq} - 1.744$ at 25 °C.

3.2. Geometry and Gibbs free energy

The neutral form of Emodin (EMH, see Fig. 1), all the deprotonated hydroxyl forms (EM^{-1}, EM^{-2} and EM^{-3}), its tautomeric isomers with the hydroxyl at position 9 (1,10- and 8,10-anthraquinones), the water molecule (H_2O), the hydroxyl (OH^-) and the hydronium (H_3O^+) ions have the geometry optimized and the vibrational frequencies calculated with quantum mechanics (QM). These calculations were performed using Density Functional Theory (DFT) [48] with the B3LYP exchange–correlation functional [49,50] and Pople basis set functions, 6-311++G(d,p) [51]. This DFT functional has produced results with a good compromise between computational cost and accuracy of the results for molecules of the anthraquinone family [17,52,53] and other organic molecules [54].

The solvent effect in the geometry was included using the polarizable continuum model (PCM) [55] with the same level of QM calculation. Hence, all geometries were obtained in vacuum and in aqueous solution. The differences found in both geometries (in gas phase and in aqueous solution) were negligible. Therefore, all the further calculations were performed in the vacuum optimized geometries.

The Gibbs free energies of all stable species, in gas phase (G_g) and in aqueous solution (G_{aq}), were calculated considering the electronic energy of the system and the corrections of zero-point energy, thermal and enthalpy at the same level of QM calculation, B3LYP/6-311++G(d,p). For the case of the proton (H^+), its gas phase free energy was obtained using the equilibrium reaction $H_2O \Longleftrightarrow OH^- + H^+$, which $\Delta G_g(H_2O \rightarrow OH^- + H^+) = G_g(OH^-) + G_g(H^+) - G_g(H_2O)$. Therefore, we determined the $G_g(H^+)$ using the experimental value of the $\Delta G_g(H_2O \rightarrow OH^- + H^+) = 385.6 \pm 0.2$ kcal/mol obtained by Bartmess and co-authors [56,57] and the calculated values of the $G_g(OH^-)$ and the $G_g(H_2O)$.

Comparing the G_{aq} of the isomers with the same quantity of deprotonation sites, we analyze the preferential position for the first and second deprotonation process of Emodin in aqueous solution. The free energy of the first deprotonation of Emodin in gas phase, ΔG_g, was calculated for both thermodynamic cycles, using Eq. (7) for the $\Delta G^{(1)}_g$ and Eq. (11) for the $\Delta G^{(2)}_g$. Additionally, to increase the numerical precision in the calculation of ΔG_g, the electronic energies of the involved species were also calculated with Møller–Plesset second order perturbation theory (MP2) [58,59] with the same basis function, MP2/6-311++G(d,p).

3.3. Free energy of solvation and pK_a

The standard solvation free energies, $\Delta G_{solv}(X)$, for X = EMH and EM^- were calculated with the Free Energy Perturbation method (FEP) [60–63], implemented in the Monte Carlo (MC) simulations [64–68]. For comparison the $\Delta G_{solv}(X)$ was also obtained with QM calculations, where the solvent effect was included using PCM, which describes the solvent as a continuum polarizable dielectric medium [55].

For the other species, $X = H^+$, H_2O and H_3O^+, several authors have studied its standard free energies of solvation in aqueous solution [34,43–45,56,69–72]. Therefore, we decided to use in this work the experimental value of the $\Delta G_{solv}(H_2O) = -6.32 \pm 0.2$ kcal/mol obtained by Ben-Naim and Marcus [70], the $\Delta G_{solv}(H_3O^+) = -110.2 \pm 0.7$ kcal/mol obtained by Pliego and Riveros [34] and the $\Delta G_{solv}(H^+) = -265.9$ kcal/mol obtained by Tissandier and co-authors [72], all in standard condition (concentration of 1.0 M in gas phase). Then, the $\Delta G_{solv}(H^+)$ and the $\Delta\Delta G_{solv}$ (water) $= \Delta G_{solv}(H_3O^+) - \Delta G_{solv}(H_2O) = -103.88$ kcal/mol were used in the calculations of the relative solvation free energy, $\Delta\Delta G^{(1)}_{solv}$ and $\Delta\Delta G^{(2)}_{solv}$ of the Schemes 1 and 2 (using Eqs. (7) and (12)), respectively.

The MC simulations were performed with the Metropolis sampling technique [73] and standard procedures as presented before [74]. The system was composed by one solute X and 500 water molecules in the isothermal-isobaric NPT ensemble, where the number of molecules N, the pressure P, and the temperature T are fixed at $N = 501$, $P = 1$ atm and $T = 25$ °C. The periodic boundary conditions and the image method were used in a cubic box that was initialized with edge of $L = 24.98$ Å and the density of 1 g/cm^3. Throughout the simulation, the geometry and potential parameters of the molecules are kept fixed, where each molecule interacts with all other molecules within a spherical region that is defined by the cutoff radius $r_c = L/2 \approx 12.5$ Å. The long-range corrections of the potential are calculated beyond this cutoff distance, as before [74]. The intermolecular interaction was described by standard Lennard–Jones plus Coulomb potential, where each interacting site i has three parameters (ε_i, σ_i and q_i), that are related by the combination rule: $\varepsilon_{ij} = (\varepsilon_i\varepsilon_j)^{1/2}$ and $\sigma_{ij} = (\sigma_i\sigma_j)^{1/2}$. The water was described with the SPC model [75] and for the solutes, EMH and EM^-, the following parameters were used: $\{\varepsilon\}$ and $\{\sigma\}$ of the OPLS force field [76] and the set of atomic charges $\{q\}$ calculated with the CHELPG procedure to fit the electrostatic potential [77] at the B3LYP/6-311++G(d,p) level of QM calculation, with the solute embedded in the solvent described by PCM. Therefore, the atomic charges of the solute include implicitly the electronic polarization due to the aqueous solutions, $\{q\}_{aq}$. This procedure, for studying properties of molecules in aqueous solution, has been shown to be better than the standard procedure of calculating the charges with HF/6-31G(d) [68,78–80]. The potential parameters (Lennard–Jones $\{\varepsilon$ and $\sigma\}$ and the atomic charges $\{q\}_{aq}$) of EMH and EM^- used in this work are shown in Supplementary Material.

As used before, the solvation free energy was obtained as the negative value of the annihilation free energy in solution, i.e. $\Delta G_{solv}(X) = -\Delta G_{annih}(X)$ [65,67,68,81]. The annihilation free energy

was calculated using a hypothetical vanishing process, $\Delta G_{annih}(X) = \Delta G(X \rightarrow 0)$, where the solute–solvent interactions are switched-off in several simulations, using the double-wide sampling technique [62,81]. In this process the initial state of the simulation is a system composed by one polarized solute in aqueous solution at 1 atm and the final state has only the solution. In other words, the solute is removed from the solution and takes it to the gas phase with the polarized set of atomic charges at 1 atm condition. Then, two additional steps should be done to obtain the correct state of the non-polarized solute in gas phase at the standard condition (concentration of 1 M). Thus, $\Delta G_{solv}(X) = -\Delta G_{annih}(X) + \Delta G_{pol}(X) + \Delta G(P_i \rightarrow P_f)$, where $\Delta G_{pol}(X)$ is the free energy variation due to the polarization process of the solute going from the gas phase to the aqueous solution and the $\Delta G(P_i \rightarrow P_f)$ is the free energy variation due to the change in the pressure of the gas phase from the standard condition (P_i = 24.46 atm) to the condition in equilibrium with the pressure of the solution (P_f = 1 atm). The $\Delta G_{pol}(X)$ involves a variation in the internal energy of the solute due to its polarization, $\Delta E_{pol}(X)$, that can be obtained by QM calculations considering the difference of the solute electronic energy with a wavefunction polarized in water with PCM (Ψ_{PCM}) and in vacuum (Ψ_o), $\Delta E_{pol}(X) = \langle \Psi_{PCM}|H_o|\Psi_{PCM}\rangle - \langle \Psi_o|H_o|\Psi_o\rangle$, where H_o is the Hamiltonian of the isolated solute. The relation $\Delta G_{pol}(X) = \Delta E_{pol}(X)$ is a good approximation considering a rigid solute. As usual [43,82], using thermodynamic relations it is obtained that $\Delta G(P_i \rightarrow P_f) = RT \ln(P_f/P_i) = -RT \ln(24.46)$.

The annihilation process was performed in three stages: first, the polarized atomic charges of the solute $\{q\}_{aq}$ were slowly reduced to zero and the negative of the solute–solvent electrostatic term of the solvation free energy, $-\Delta G_{ele}(X)$, was calculated; then, the attractive term of the Lennard-Jones potential, r^{-6}, was vanished and the negative of the van der Waals term of the solvation free energy, $-\Delta G_{vdW}(X)$, was calculated; and finally, the repulsive term of the Lennard–Jones potential, r^{-12}, was also vanished and the negative of the cavitation term of the solvation free energy, $-\Delta G_{cav}(X)$, was calculated.

Then, the total value of the standard solvation free energy of each species was obtained as:

$$\Delta G_{solv}(X) = \Delta G_{ele}(X) + \Delta G_{vdW}(X) + \Delta G_{cav}(X) + \Delta G_{pol}(X) - RT \ln(24.46) \quad (14)$$

where the first three terms were calculated with FEP-MC simulation [65,66,83] and takes into account only the solute–solvent (intermolecular) interaction, the $\Delta G_{pol}(X)$ were calculated with PCM and consider the changes of the solute (intramolecular) due to its polarization process in going from the gas phase to the solution, and the last term, $-RT \ln(24.46)$, is equal to 1.9 kcal/mol at 25 °C and consider the change in the ideal gas at the standard concentration of 1 M to the condition of 1 atm in equilibrium with the solution.

The series of MC simulations was composed by a total of twenty simulations performed to make the solute *X* disappears slowly from the solution in three stages: (i) 12 simulations with double-wide sampling were performed to annihilate the Coulomb potential, $\lambda_i\{q\}_{aq}$, with λ_i = 1.000 ← 0.975 → 0.950, 0.950 ← 0.925 → 0.900, 0.9000 ← 0.875 → 0.850, 0.850 ← 0.825 → 0.800, 0.800 ← 0.775 → 0.750, 0.750 ← 0.725 → 0.0700, 0.700 ← 0.675 → 0.650, 0.650 ← 0.625 → 0.600, 0.600 ← 0.550 → 0.500, 0.500 ← 0.450 → 0.400, 0.400 ← 0.350 → 0.300, 0.300 ← 0.200 → 0.00; (ii) 4 simulations with double-wide sampling to annihilate the attractive term of the LJ potential with λ_i = 1.000 ← 0.875 → 0.750, 0.750 ← 0.625 → 0.500, 0.500 ← 0.375 → 0.250, 0.250 ← 0.125 → 0.00; and (iii) 4 simulations without double-wide sampling to annihilate the repulsive term of the LJ potential with λ_i = 1.00 → 0.75, 0.75 → 0.50, 0.50 → 0.25, 0.25 → 0.00. For each λ, five independent simulations with double-wide sampling were performed to calculate the average and the standard deviation of the free energy between the states $\lambda_i \rightarrow \lambda_{i+1}$ and $\lambda_i \rightarrow \lambda_{i-1}$. Each simulation was divided in two large stages, thermalization and equilibrium, both with 1.5×10^8 MC steps. More details about this procedure can be found in Refs. [64,65].

For comparison the standard solvation free energies, ΔG_{solv}(EMH) and $\Delta G_{solv}(EM^-)$, were also carried out using the PCM with the United Atom for Hartree Fock (UAHF) model for the cavity shape at HF/6-31+G(d) level of calculation [84]. Many works have shown that this HF/6-31+G(d)/PCM/UAHF level provides reliable standard solvation free energies of neutral and charged molecules giving results in excellent agreement with experimental data, due to the internal parametrization of the non-electrostatic terms of the free energy in the PCM method [85–87]. In this calculation the electrostatic term of the solvation free energy, $\Delta G_{ele}(X)$, already includes the solute polarization term, $\Delta G_{pol}(X)$, because it takes into account the inter and intramolecular interaction. To better compare the values obtained with PCM and FEP-MC, we presented these two terms separately (in Section 4.4) and adding both terms one can get the total electrostatic term of the solvation free energy.

All QM calculations were performed with Gaussian 03 program [88] and the MC simulations and FEP calculations with DICE program [89].

4. Results and discussions

4.1. Experimental UV/Visible spectrophotometric titration and pK_a

Before setting the assay of Emodin in water, we performed the experimental measures of the UV/Visible absorption spectra of the Emodin in water–methanol mixture (1:3 v/v) at concentration of 0.025 mM varying the apparent *pH* from 12.66 to 2.09. This mixture is simpler than the aqueous solution because no aggregation of the Emodin was observed. In Fig. 2 the UV/Visible spectra of

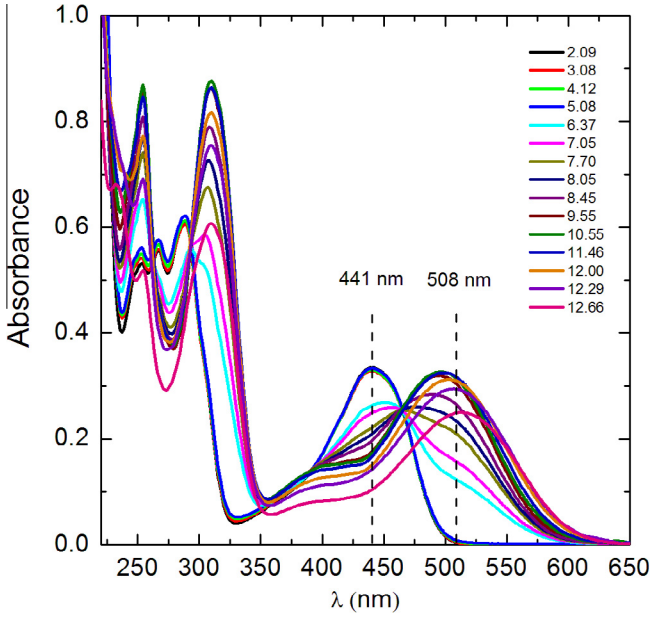

Fig. 2. The effect of the apparent *pH* on the UV/Visible absorption spectra of the Emodin in water–methanol mixture (1:3 v/v) at concentration of 0.025 mM. The vertical dashed lines show the λ_{max} of the first band of the Emodin in alkaline mixture, *pH* = 12.66, at 508 nm and in acidic mixture, *pH* < 5.08, at 441 nm.

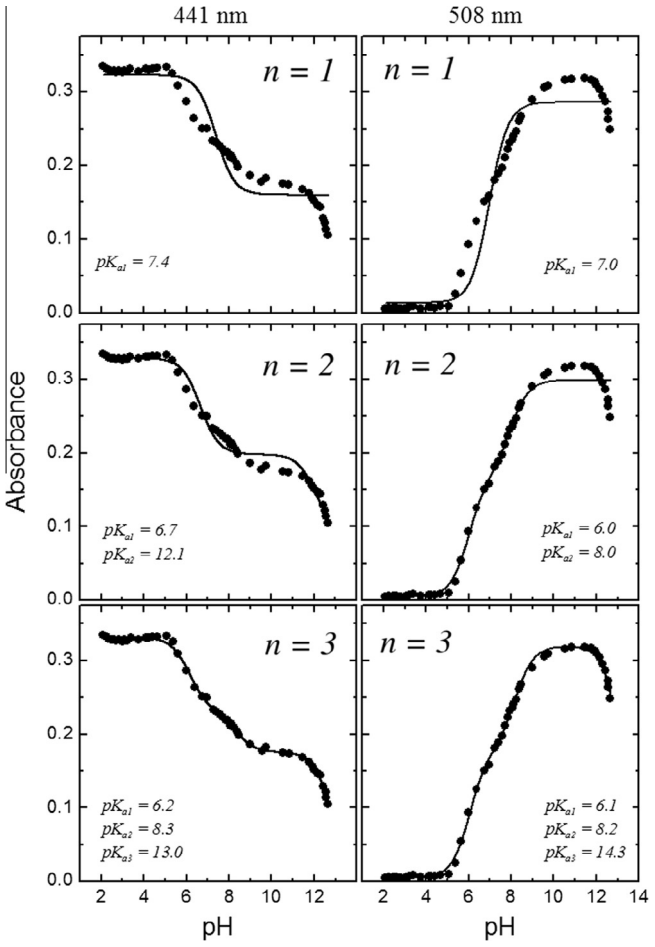

Fig. 3. (symbols) The Emodin absorbance at two wavelengths, 441 nm (left) and 508 nm (right), versus the apparent *pH* of the water–methanol mixture and (line) the best fit of the Eq. (5) with one term of the sum ($n = 1$, top), two term of the sum ($n = 2$, middle) and three terms of the sum ($n = 3$, bottom).

the Emodin in the mixture are shown for 15 illustrative samples selected in the studied *pH* range.

As it can be seen the absorption spectrum of Emodin is very sensitive to the *pH* variation. The first absorption band changes its maximum absorbance from 508 nm to 441 nm when the apparent *pH* varies from 12.66 to 2.09. This is in agreement with previous measurements performed by Pal and Jana [16].

We selected these two wavelengths, 508 and 441 nm, to perform the UV/Visible ST curves and used Eq. (5) to obtain the pK_{ai}, (see Fig 3). Considering only one deprotonation process in the entire range of the *pH* ($n = 1$ in Eq. (5)), we obtained $pK_{a1} = 7.4$ at 441 nm and $pK_{a1} = 7.0$ at 508 nm. These values are in agreement with the value of 7.2 obtained previously by Pal and Jana [16] in the same mixture proportion of water–methanol by Bjerrum's method. However, in Fig. 3 (top) it is easy to see that the best fit of Eq. (5) with only one term of the sum does not adjust well the experimental data. Then, we try also to fit the Eq. (5) with $n = 2$ and 3, i.e. assuming two or three decoupled and non-interacting deprotonation sites of the Emodin in the mixture at the *pH* range between 12.66 and 2.09. These two additional fitting of Eq. (5) are also presented in Fig. 3 (middle and bottom). For $n = 2$ (see Fig. 3, middle), we obtained $pK_{a1} = 6.7$ and $pK_{a2} = 12.1$ at 441 nm, and $pK_{a1} = 6.0$ and $pK_{a2} = 8.0$ at 508 nm and for $n = 3$ (see Fig. 3, bottom), we obtained $pK_{a1} = 6.2$, $pK_{a2} = 8.3$, $pK_{a3} = 13.0$ at 441 nm and $pK_{a1} = 6.1$, $pK_{a2} = 8.2$, $pK_{a3} = 14.3$ at 508 nm. Perusal of Fig. 3 shows that the best fitting of the experimental data is obtained assuming the existence of three acidity constants in the studied range of *pH*. Furthermore, the values of pK_{a1} and pK_{a2} obtained for the two different wavelengths are equivalent when the three deprotonations were assumed. Since our measurements were performed with *pH* up to 12.66, the values obtained for pK_{a3} (13.0 and 14.3) are in the limiting of the *pH* range used. Therefore, we believe that the pK_{a3} values are not reliable, but we are confident that our best values for the apparent acidity constants of the Emodin in water–methanol mixture (1:3 v/v) are $pK_{a1} = 6.2 \pm 0.1$, $pK_{a2} = 8.3 \pm 0.1$ and $pK_{a3} > 12.7$.

This new analysis of the experimental titration curve gives a different conclusion compared with that one obtained by Pal and Jana [16]. However, it seems to be more adequate to the picture of a stepwise dissociation of the protons of the three-hydroxyl groups existent in Emodin. Then, we conclude that the Emodin in water–methanol mixture (1:3 v/v), from *pH* 2.09 to 12.66, loses two protons, going from the neutral form to the charged divalent anionic form, with apparent acidity constants of 6.2 and 8.3. The acidity constant of the third deprotonation is larger than 12.7.

For completeness, we tested two additional fittings of the Eq. (5), with $n = 4$ and 5. With these new fittings, we obtained: (i) the same values of the pK_{a1} and pK_{a2} as obtained with $n = 3$; (ii) the values of the pK_{a3} with small variation for the two analyzed wavelength ($pK_{a3} = 14.4 \pm 0.1$); (iii) negative values for the pK_{a4} and pK_{a5}; and (iv) a negligible improvement in the agreement with the experimental data. Thus, we conclude that the best fitting of the titration curve with the Eq. (5) was obtained with $n = 3$.

In the case of the aqueous solution, the experiment titration curve was obtained by the UV/Visible absorption spectra of the Emodin decreasing the sample *pH* value from 13.8 to 2.0. Around 70 UV/Visible spectra were measured in this *pH* range at each different concentration (0.1 and 0.025 mM). Due to the Emodin aggregation and the precipitation at lower *pH* values, samples were strongly vortexed immediately before each optical assay. In Fig. 4a the UV/Visible spectra of the Emodin in water are shown for 11 illustrative samples selected in the studied *pH* range. They show a large dependence of the optical absorption spectrum of the Emodin on the *pH* of the medium. At higher *pH* values, the Emodin is deprotonated and charged, and the sample is clear and reddish. As the *pH* goes down, the color of the sample changes, untill it gets yellow at low *pH* values. Below *pH* = 8, Emodin aggregates, precipitating after around one minute. In Fig. 4a, at *pH* values 7.71, 7.02, 4.40 and 2.0, the presence of the Emodin aggregates is evidenced by the scattering profile underneath the optical absorption spectrum (light scattering depends on wavelength as λ^{-x}, where x depends on the scattering particle dimensions [90]). Due to the presence of the absorption bands, it is not possible to precisely subtract the light scattering from the Emodin absorption spectrum. Therefore, each spectrum was roughly corrected by subtracting the absorbance value at 650 nm. This correction assumes that there is no electronic absorption transition of the Emodin in the region near 650 nm, and then the absorbance is zero. The corrected spectra are shown in Fig. 4b.

The dependence of the absorbance at 519 and 308 nm (see Fig. 4b) with respect to the *pH* leads to the UV/Visible ST curves shown in Fig. 5. These wavelength values are the maxima of the first two bands at $pH > 11$. The best fit of those UV/Visible ST curves by Eq. (5) yield to two acidity constants, pK_{a1} and pK_{a2}, for the Emodin in aqueous solution. The fitting with three acidity constants does not improve significantly the agreement with the experimental data of the titration curve. So then, we decided to stay with the simpler adjustment with two terms (Eq. (5) with $n = 2$). For both wavelengths, the best fitted values for the first and second acidity constants were similar. Therefore, the best values for the acidity constants are $pK_{a1} = 8.0 \pm 0.1$ and $pK_{a2} = 10.9 \pm 0.2$. These values are the average and error for four

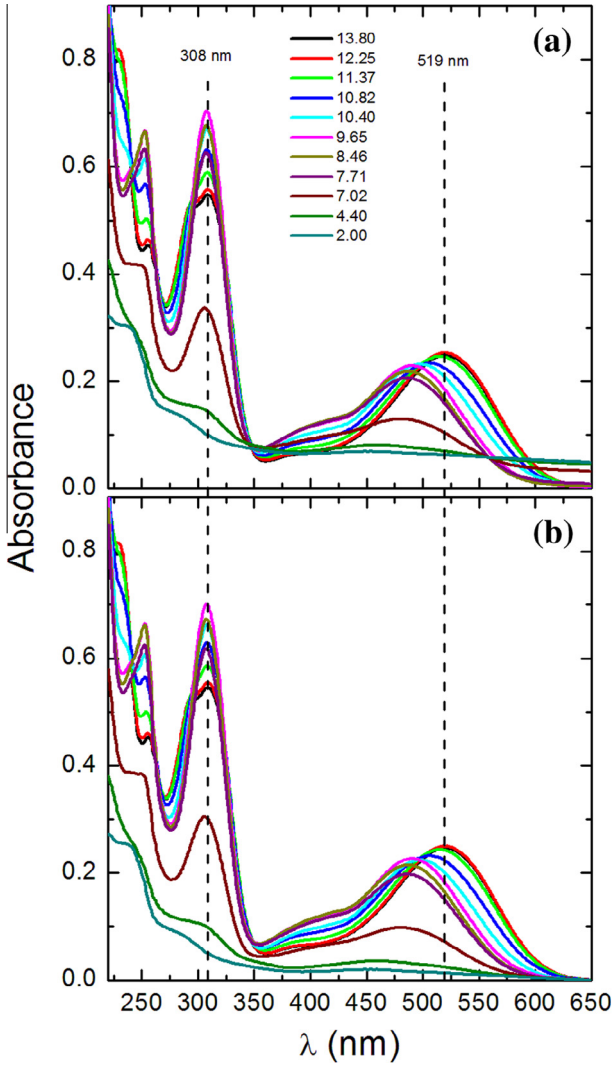

Fig. 4. The effect of the *pH* on the UV/Visible absorption spectra of the Emodin in aqueous solution at concentration of 0.025 mM, without corrections (a) and with light scattering correction (b). The vertical dashed lines show the λ_{max} of the first and second bands of the Emodin in alkaline solution, $pH > 11$, at 519 and 308 nm, respectively.

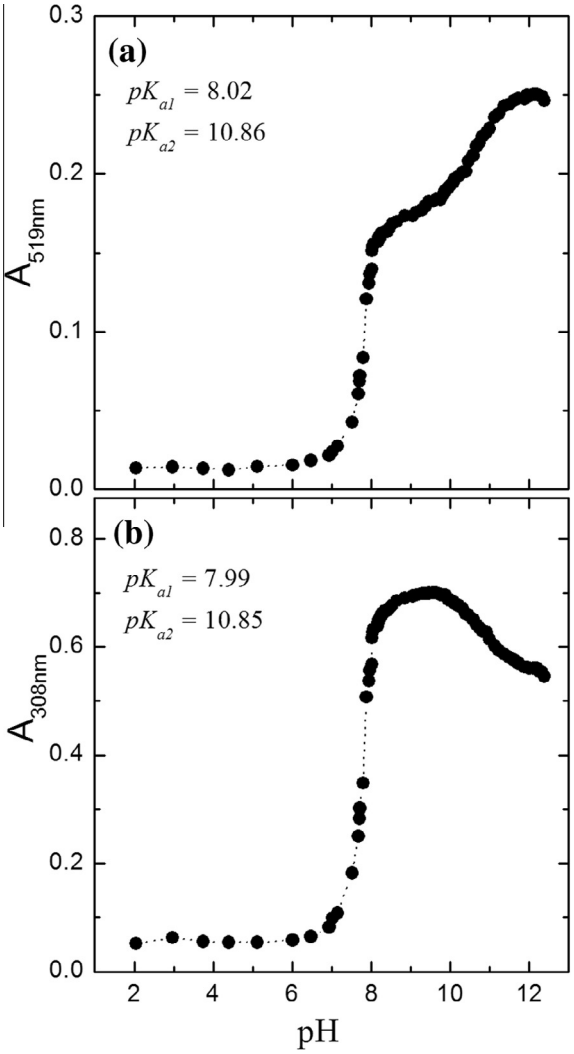

Fig. 5. The effect of the *pH* on the Emodin absorbance values (corrected by the light scattering, see text) at 519 and 308 nm with concentration of 0.025 mM. The pK_a values were obtained from the best fitting of Eq. (5) with two terms ($n = 2$).

different experiments, two experiments for each concentration of 0.025 and 0.100 mM of the Emodin.

The reason for assaying different Emodin concentrations was to test whether the formation of Emodin aggregates or the presence of light scattering would affect the best fitted pK_a values. However, the great similarity among the results obtained with different Emodin concentrations and at different wavelengths reinforce the accuracy of the pK_{a1} and pK_{a2} values, i.e. the first deprotonation of the Emodin in aqueous solution at $pK_{a1} = 8.0 \pm 0.1$ and second deprotonation at $pK_{a2} = 10.9 \pm 0.2$. According to Eq. (9), these pK_a values give a standard first and second deprotonation free energy of the Emodin in water as 10.9 ± 0.2 kcal/mol and 14.9 ± 0.3 kcal/mol, respectively. Note that the Emodin aggregates are detected bellow the value of pK_{a1}, where there is a predominance of the neutral Emodin, EMH. Therefore, the Emodin in aqueous solution, from *pH* 2.0 to 13.8, loses two protons, going from the neutral form to the charged divalent form, with acidity constants of 8.0 and 10.9. The acidity constant of the third deprotonation is out of the *pH* range studied here, i.e. larger than 13.8. Our best value of 8.0 ± 0.1 for the pK_{a1} of the Emodin in water is in agreement with the value showed in the graphic of Fig. 4 of the Ref. [30]. This graphic shows the effect of the acetonitrile concentration on the pK_a values of five molecules of the anthraquinone family in water–acetonitrile mixture. In the case of Emodin, the point at 0% of acetonitrile gives a pK_a of ~8.2 for Emodin in water.

4.2. Geometry optimization and relative stability of the isomers

Initially we performed geometry optimization for the isolated molecules in vacuum with the B3LYP/6-311++G(d,p) level of calculation. The optimized systems were: the neutral Emodin, all the deprotonated hydroxyl forms and the tautomeric isomers with the hydroxyl at position 9, i.e. the 1,10- and 8,10-anthraquinone tautomeric forms. We found, as stable structures, only the 9,10-anthraquinone neutral form, 6 anionic/deprotonated forms of Emodin, in which 3 of them presented one deprotonation site, 2 presented two deprotonation sites and 1 presented three deprotonation sites. These forms are: **3,8-EM**$^-$ (9,10-anthraquinone with deprotonation at position 1 and two hydroxyl groups at positions 3 and 8), **1,8-EM**$^-$ (9,10-anthraquinone with deprotonation at position 3 and two hydroxyl groups at positions 1 and 8), **1,3-EM**$^-$ (9,10-anthraquinone with deprotonation at position 8 and two hydroxyl groups at positions 1 and 3), **1-EM**$^{2-}$ (9,10-anthraquinone with deprotonation sites at positions 3 and

Table 1
The electronic energy (E_g in kcal/mol), free energy (G_g in kcal/mol) and the dipole moment (μ_g in D) of the Emodin forms X in vacuum using B3LYP/6-311++G(d,p) level of QM calculation. In aqueous solution, the free energies (G_{aq}) and the dipole moment (μ_{aq}) were obtained using the solvent described by PCM with the same level of calculation. The relative values, Δ, are also shown, comparing the isomer with the same quantity of deprotonation sites (for one site the reference was the **1,8-EM**$^-$ and for two was the **1-EM**$^{2-}$). The dipole moments for the anionic forms were calculated with the origin at the center of the nuclear changes.

X	E_g	G_g	G_{aq}	μ_g	μ_{aq}
EMH	−598676.30	−598565.89	−598572.34	2.68	3.49
3,8-EM$^-$	−598331.83	−598232.14	−598281.32	8.47	12.91
1,8-EM$^-$	−598348.98	−598247.08	−598287.28	10.44	15.33
1,3-EM$^-$	−598331.78	−598230.96	−598280.93	7.12	11.36
Δ (1,8-EM$^-$ **→ 3,8-EM**$^-$**)**	17.15	14.94	5.96		
Δ (1,8-EM$^-$ **→ 1,3-EM**$^-$**)**	17.20	16.12	6.35		
1-EM^{2-}	−597932.60	−597840.54	−597990.00	8.04	12.17
9-EM^{2-}	−597925.15	−597832.27	−597984.38	12.78	19.46
Δ (1-EM^{2-} **→ 9-EM**$^{2-}$**)**	7.45	8.27	5.62		
EM^{3-}	−597426.91	−597343.98	−597681.60	13.81	21.68

8 and one hydroxyl group at position 1), **9-EM**$^{2-}$ (8,10-anthraquinone with deprotonation sites at positions 1 and 3 and one hydroxyl group at position 9) and **EM**$^{3-}$ (deprotonation sites at positions 1, 3 and 8). The electronic energy, Gibbs free energy and dipole moment of those stable structures in vacuum are shown in Table 1.

All the optimized geometries were found to be planar and having intramolecular hydrogen bonds with oxygen O9, in good agreement with the geometries obtained with DFT, B3LYP/6-31+G(d,p) [17] and B3LYP/6-311++G(d,p) [53], and with the crystallographic experimental data of 1,8-dihydroxyanthraquinone [91,92]. We identified that none of the following tautomeric forms of Emodin are stable, at the B3LYP/6-311++G(d,p) level, considering the neutral form of the 1,10-anthraquinone and 8,10-anthraquinone; with one deprotonation site: **1,9-EM**$^-$ (8,10-anthraquinone with the hydroxyl groups at positions 1 and 9), **3,9-EM**$^-$ (1,10-anthraquinone and 8,10-anthraquinone with the hydroxyl groups at positions 3 and 9) and **8,9-EM**$^-$ (1,10-anthraquinone with the hydroxyl groups at positions 8 and 9); and two deprotonation sites: **8-EM**$^{2-}$ (1,10-anthraquinone and 9,10-anthraquinone with one hydroxyl group at position 8). Starting the geometry optimization with any one of these tautomeric forms, they spontaneously became one of the stable forms shown in Table 1. Therefore, our results do not support the existence of an equilibrium structure for the 1,10-anthraquinone and 8,10-anthraquinone tautomeric forms of neutral Emodin in vacuum and in aqueous solution. Then, these tautomers do not contribute to any property of Emodin in these two environments. This result is in agreement with the one obtained by Nguyen and co-authors [17], that could not obtain an equilibrium geometry for the 1,10-anthraquinoid tautomer of Emodin in vacuum or in ethanol.

In Table 1, comparing the free energy in gas phase, G_g, of the three isomeric forms with one deprotonation, **3,8-EM**$^-$, **1,8-EM**$^-$ and **1,3-EM**$^-$, the isomer with deprotonation at position 3 (**1,8-EM**$^-$) is the most stable compared with the others, ΔG_g(**1,8-EM**$^-$ → **3,8-EM**$^-$) = 14.9 kcal/mol and ΔG_g(**1,8-EM**$^-$ → **1,3-EM**$^-$) = 16.1 kcal/mol. The larger contribution for this stabilization comes from the electronic energy (ΔE_g(**1,8-EM**$^-$ → **3,8-EM**$^-$) = 17.1 kcal/mol and ΔE_g(**1,8-EM**$^-$ → **1,3-EM**$^-$) = 17.2 kcal/mol). Although the energies corrections (sum of zero-point, thermal and enthalpy) obtained after the vibration frequencies calculations are large (around 100 kcal/mol, see $G_g - E_g$ in Table 1), the differences between the isomers are small, around 1.5 kcal/mol.

Comparing the free energy in aqueous solution, G_{aq}, the isomer **1,8-EM**$^-$ remains more stable by 5.9 kcal/mol compared to **3,8-EM**$^-$ and 6.3 kcal/mol compared to **1,3-EM**$^-$. This large difference in the free energy of the isomers in aqueous solution leads to an equilibrium system with only the **1,8-EM**$^-$ isomer at room temperature ($RT \approx 0.6$ kcal/mol). Thus, we conclude that the first deprotonation of the Emodin takes place at position 3 and for further calculations of the free energy of solvation and pK_a, only this isomer was considered, i.e. EM$^-$ = **1,8-EM**$^-$. Analyzing the divalent anionic forms, the isomer **1-EM**$^{2-}$ is 5.6 kcal/mol more stable than the isomer **9-EM**$^{2-}$. Therefore, we conclude that the second deprotonation of Emodin in water takes place at position 8. Our results for the location of the first (at position 3) and second (at position 8) deprotonation process of Emodin in aqueous solution obtained with QM calculation are in agreement with the stepwise proton dissociation proposed by Pal and Jana [16].

It is interesting to note that the aqueous environment maintains the same stability of these isomers in the gas phase. But the environment plays a significant rule in the charge redistribution and electronic polarization of the anionic/deprotonated forms that can be seen in the large difference between the dipole moment in vacuum (μ_g) and in aqueous solution (μ_{aq}). There is an increase of 50–60% of the dipole moment of the deprotonated forms of Emodin in water compared to vacuum. Analyzing the atomic charge of the molecules in vacuum and in water, we identify that in general there is an increase in the modules of the charges calculated in water. However, this increase in not uniform. In the case of neutral form, EMH, the three oxygen atoms of the hydroxyl groups (O1, O3 and O8) have almost the same charge (around −0.63 in vacuum and −0.68 in water, an increase of ∼8%). However the two oxygen atoms of the carbonyl groups (O9 and O10) have distinct charges (−0.64 and −0.49 in vacuum and −0.67 and −0.57 in water, an increase of 5% in O9 and 16% in O10) due to the two intramolecular hydrogen bonds formed between O1H1 and O8H8 with O9. In the case of the first deprotonated form, 1,8-EM$^-$, the three oxygen atoms of the hydroxyl groups have almost the same charge in vacuum (around −0.71), but became distinct in water leaving the deprotonated oxygen more negative than the others (around −0.72 for O1 and O8 and −0.84 for O3). Thus, we identified that the solvent effect on the electronic polarization of this type of molecules is important and cannot be neglected for a good description of its interaction with the solvent. For this reason, we used a set of polarized atomic charges, $\{q\}_{aq}$, in the simulations of EMH and EM$^-$ in water.

For further consideration, the variation in the internal energies of the EMH and EM$^-$ due to their polarization in the presence of a water reaction field, $\Delta E_{pol}(X)$ (see Section 3.3 for computational details), were calculated as 2.1 and 4.5 kcal/mol, respectively. The value of the $\langle \Psi_{PCM}|H_o|\Psi_{PCM}\rangle$ term was obtained in the same QM calculation as the $_{aq}$ and ΔG_{aq} (shown in Table 1) and the value of the $\langle \Psi_o|H_o|\Psi_o\rangle$ term was obtained in the vacuum QM calculation. These values were used in the polarization free energy, $\Delta G_{pol}(X)$, that will be discussed in the following sections.

4.3. Theoretical deprotonation process in gas phase

The gas phase free energy of the first deprotonation of the Emodin, ΔG_g was calculated using the free energy of the involved

Table 2
The free energy in vacuum (in kcal/mol) for the species involved in the deprotonation process of water and Emodin in gas phase. The geometries were optimized with B3LYP/6–311++G(d,p) and the corrections of zero-point, thermal and enthalpy were obtained after the vibrational frequencies calculations. The electronic energies were calculated with two different methods: B3LYP and MP2 with the same basis function.

Free energy in gas phase, G_g	B3LYP	MP2
$G_g(H_2O)$	−47976.17	−47860.70
$G_g(H_3O^+)$	−48140.08	−48025.93
$G_g(OH^-)$	−47587.29	−47469.68
$\Delta G_g(2H_2O \rightarrow OH^- + H_3O^+)$	224.97	225.80
$\Delta G_g(2H_2O \rightarrow OH^- + H_3O^+)$ Experimental[a]	226.0 ± 0.2	
$\Delta G_g(H_2O \rightarrow OH^- + H^+)$ Experimental[b]	385.6 ± 0.2	
$G_g(H^\star) = \Delta G_g(H_2O \rightarrow OH^- + H^+) + G_g(H_2O) - G_g(OH^-)$	−3.3 ± 0.2	−5.4 ± 0.2
$\Delta G_g(\text{Water}) = G_g(H_3O^+) - G_g(H_2O)$	−163.91	−165.23
$G_g(\text{EMH})$	−598565.89[c]	−596948.38
$G_g(EM^-) = G_g(1,8\text{-}EM^-)$	−598247.08[c]	−596628.10
$\Delta G_g(\text{Emodin}) = G_g(EM^-) - G_g(\text{EMH})$	318.81	320.28
$\Delta G_g^{(1)} = \Delta G_g(\text{Emodin}) + G_g(H^\star)$	315.5 ± 0.2	314.9 ± 0.2
$\Delta G_g^{(2)} = \Delta G_g(\text{Emodin}) + \Delta G_g(\text{Water})$	154.9 ± 0.2	155.1 ± 0.2

[a] Value obtained from Refs. [34,44].
[b] Value obtained from Refs. [56,57].
[c] The same values presented in Table 1.

species as shown in Eqs. (7) and (11). For completeness, the calculations of the gas phase deprotonation free energy of water, $\Delta G_g(H_2O \rightarrow OH^- + H^+)$ and $\Delta G_g(2H_2O \rightarrow OH^- + H_3O^+)$, were also calculated and compared with the best experimental values of 385.6 ± 0.2 kcal/mol [56,57] and 226.0 ± 0.2 kcal/mol [34,44], respectively.

The free energy of each species in vacuum was calculated with B3LYP/6-311++G(d,p) adding the electronic energy with the corrections of zero-point, thermal and enthalpy. Except for the H^+, which we used the equilibrium reaction $H_2O \Longleftrightarrow OH^- + H^+$ to obtain the $G_g(H^\star)$. Additionally, to increases the numerical precision of the free energy values, the calculations of the electronic energies were improved using MP2 method with the same basis set. These values are shown in Table 2.

The calculated values of the $\Delta G_g(2H_2O \rightarrow OH^- + H_3O^+)$ is 225.8 (224.9) kcal/mol with MP2 (B3LYP). These values are in very good agreement with the experimental value of 226.0 ± 0.2 kcal/mol [34,44]. We obtained the $G_g(H^+)$ as −5.4 (−3.3) kcal/mol with MP2 (B3LYP), using the experimental value of $\Delta G_g(H_2O \rightarrow OH^- + H^+)$ = 385.6 ± 0.2 kcal/mol and the calculated values of $G_g(H_2O)$ and the $G_g(OH^-)$. For further calculations, we adopted the MP2 values as our best results, $\Delta G_g(\text{water})$ = −165.2 ± 0.2 kcal/mol, $G_g(H^\star)$ = −5.4 ± 0.2 kcal/mol, $\Delta G_g^{(1)}$ = 314.9 ± 0.2 kcal/mol using Eq. (7) and $\Delta G_g^{(2)}$ = 155.1 ± 0.2 kcal/mol using Eq. (11).

4.4. Theoretical free energy of solvation and pK_a

The three terms of the standard solvation free energies, $\Delta G_{ele}(X)$, $\Delta G_{vdW}(X)$, $\Delta\Delta G_{cav}(X)$, for X = EMH and EM^-, in aqueous solution were calculated using FEP-MC simulations, as presented in Section 3.3. Five independent sets of simulations were performed and the final values and standard deviations were evaluated (shown in Table 3). Each set was composed by 20 simulations: 12 simulations for vanishing the electrostatic term of the solute–solvent interactions and calculating the $\Delta G_{ele}(X)$; 4 simulations for vanishing the attractive part of the Lennard–Jones term of the solute–solvent interactions and calculating the $\Delta G_{vdW}(X)$; and 4 simulations for vanishing the repulsive part of the Lennard–Jones term of the solute–solvent interactions and calculating the $\Delta G_{cav}(X)$. The polarization free energies, $\Delta G_{pol}(X)$, were calculated as 2.1 and 4.5 kcal/mol for EMH and EM^-, respectively (see Sections 3.3 and 4.2). Then, using Eq. (14) the value of $\Delta G_{solv}(X)$ were obtained; using Eqs. (8) and (12) the values of $\Delta\Delta G_{solv}$(Emodin), $\Delta\Delta G_{solv}$(water), $\Delta\Delta G_{solv}^{(1)}$ and $\Delta\Delta G_{solv}^{(2)}$ were obtained; using Eqs. (6) and (10) the values of $\Delta G_{aq}^{(1)}$ and $\Delta G_{aq}^{(2)}$ were obtained; and finally, using Eqs. (9) and (13) the values of pK_{a1} were obtained. All these values are shown in Table 3. For comparison, the four terms of the standard solvation free energies were also calculated using PCM with UAHF model for the cavity shape at HF/3-61+G(d). These values are also shown in Table 3, in parenthesis.

The total electrostatic term of the solvation free energies, $\Delta G_{total\text{-}ele}(X) = \Delta G_{ele}(X) + \Delta G_{pol}(X)$, are −8.1 (−15.2) kcal/mol for EMH and −43.9 (−52.8) kcal/mol for EM^- using FEP-MC model (PCM). We observed an agreement in the tendency of both solvent models: FEP-MC model where the solvent molecules are explicitly included in the calculation, and the PCM where the solvent is treated as a polarizable continuum medium. However, comparing the non-electrostatic terms, $\Delta G_{total\text{-}nonele}(X) = \Delta G_{vdW}(X) + \Delta G_{cav}(X) - RT$

Table 3
Standard solvation free energies in (kcal/mol) of the species involved in the first deprotonation process of the Emodin in water following the equilibrium reaction shown in Schemes 1 and 2. The values were calculated using FEP-MC simulation and in parenthesis using QM calculation with HF/6-31+G(d)/PCM/UAHF.

Free Energy	X = EMH	$X = EM^-$	Relative values (EM^- - EMH)
$\Delta G_{ele}(X)$	−10.2 ± 0.2 (−17.1)	−48.4 ± 0.2 (−57.2)	−38.2 ± 0.2 (−40.1)
$\Delta G_{vdW}(X)$	−20.0 ± 0.4 (−27.0)	−20.6 ± 0.3 (−26.7)	−0.6 ± 0.5 (0.3)
$\Delta G_{cav}(X)$	11.9 ± 0.6 (30.7)	11.4 ± 0.6 (30.5)	−0.5 ± 0.6 (−0.2)
$\Delta G_{pol}(X)$	2.1 (1.8)	4.5 (4.4)	2.4 (2.6)
−RT ln(24.46)	−1.9	−1.9	0.0
$\Delta G_{total\text{-}ele}(X)$	−8.1 ± 0.2 (−15.3)	−43.9 ± 0.2 (−52.8)	−35.8 ± 0.2 (−37.5)
$\Delta G_{total\text{-}nonele}(X)$	−10.0 ± 0.7 (3.7)	−11.1 ± 0.7 (3.8)	−1.1 ± 0.7 (0.1)
$\Delta G_{solv}(X)$	−18.1 ± 0.7 (−11.6)	−55.0 ± 0.7 (−49.0)	$\Delta\Delta G_{solv}$(Emodin) = −36.9 ± 1.4 (−37.4 ± 1.0)
	$X = H_2O$	$X = H_3O^+$	
$\Delta G_{solv}(X)$	−6.3 ± 0.2[a]	−110.2 ± 0.7[b]	$\Delta\Delta G_{solv}$(Water) = −103.9 ± 0.7 $\Delta G_{solv}(H^+)$ = −265.9 ± 0.2[c]
	$\Delta\Delta G_{solv}^{(i)}$	$\Delta G_g^{(i)}$[d]	$\Delta G_{aq}^{(i)}$
i = Scheme 1	−302.8 ± 1.4 (−303.3 ± 1.0)	314.9 ± 0.2	12.1 ± 1.4 (11.6 ± 1.0)
i = Scheme 2	−140.8 ± 1.4 (−141.3 ± 1.0)	155.1 ± 0.2	14.3 ± 1.4 (13.8 ± 1.0)
pK_{a1}	8.8 ± 0.9 (8.5 ± 0.7) from $\Delta G_{aq}^{(1)}$[e]		8.0 ± 0.1 Our exp. result
	8.7 ± 0.9 (8.4 ± 0.7) from $\Delta G_{aq}^{(2)}$[f]		

[a] Value obtained from Ref. [70].
[b] Value obtained from Ref. [34].
[c] Value obtained from Ref. [72].
[d] MP2 values of Table 2.
[e] Using Eq. (9).
[f] Using Eq. (13).

ln(24.46), we identified a discrepancy between the two models, −10.0 (3.7) kcal/mol for EMH and −11.1 (3.8) kcal/mol for EM^- using FEP-MC simulations (PCM). For the explicit solvent model the contribution of the non-electrostatic term is negative, around 10–11 kcal/mol, but for the continuum solvent model this term is positive, around 4 kcal/mol. These difference between the two models appears clearly in the total values of the standard solvation free energy of each species, ΔG_{solv}(EMH) = −18.1 ± 0.7 (−11.6) kcal/mol and $\Delta G_{solv}(EM^-)$ = −55.0 ± 0.7 (−49.0) kcal/mol, for FEP-MC model (PCM). On the other hand, this difference of the two solvent models does not appear in the relative free energy of solvation, $\Delta\Delta G_{solv}$ (Emodin) = $\Delta G_{solv}(EM^-) - \Delta G_{solv}$(EMH) = −36.9 ± 1.4 (−37.4 ± 1.0) kcal/mol, and in the standard deprotonation free energy of Emodin in aqueous solution by the direct dissociation $\Delta G_{aq}^{(1)}$ = 12.1 ± 1.4 (11.6 ± 1.0) kcal/mol using Scheme 1 and by the acid-base reaction with water $\Delta G_{aq}^{(2)}$ = 14.3 ± 1.4 (13.8 ± 1.0) kcal/mol using Scheme 2. The difference between these values obtained with FEP-MC and PCM is less than 1.0 kcal/mol and this is caused by the cancelation of the non-electrostatic term of EMH and EM^- that are very similar. Finally, we should mention an excellent agreement between the calculated pK_{a1} values of the Emodin in aqueous solution, 8.8 ± 0.9 (8.5 ± 0.7) using Scheme 1 and 8.7 ± 0.9 (8.4 ± 0.7) using Scheme 2, with FEP-MC (PCM) and the experimental data obtained from the UV/Visible spectrophotometric titration curves, 8.0 ± 0.1.

5. Conclusions

We obtained the first and second pK_a values of the Emodin in aqueous solution using the UV/Visible spectrophotometric titration curves, pK_{a1} = 8.0 ± 0.1 and pK_{a2} = 10.9 ± 0.2. The UV/Visible absorption spectra of the Emodin were measured in a *pH* interval of ∼13 to 2. We observe aggregation of the Emodin at *pH* < 7.5. The samples were homogenized by strongly vortexing immediately before each measurement. For analyzing the existence of the aggregation effects in the obtained pK_a values, the measurements were performed in two concentrations, 0.100 and 0.025 mM, and the titration curves were analyzed in two wavelengths, 519 and 308 nm. Our results showed to be robust and present insignificant influence due to the aggregation of the Emodin in lower *pH*. Therefore, we are confident on the accuracy of these pK_a values.

Additionally, we obtained the pK_a values of the Emodin in the water–methanol mixture (1:3 v/v) using the same procedure. No aggregation of the Emodin was observed. For this system, we put forward a new interpretation for the experimental data. Using the hypothesis of only one deprotonation of the Emodin in this mixture at the *pH* interval of ∼13 to 2, we obtained the result of apparent pK_{a1} = 7.4 with the titration curve fitting at 441 nm and pK_{a1} = 7.0 at 508 nm, in good agreement with the value of 7.2 obtained previously by Pal and Jana [16]. However, the experimental data were not well adjusted by the fitting (see Fig. 3). Then, using a hypothesis of three deprotonations of the Emodin, we obtained the experimental data well fitted by Eq. (5), and the apparent acidity constants are pK_{a1} = 6.2 ± 0.1, pK_{a2} = 8.3 ± 0.1 and pK_{a3} > 12.7 for the Emodin in water–methanol mixture (1:3 v/v).

Performing quantum mechanics calculations (B3LYP and MP2 with 6-311++G(d,p)) for all possible deprotonation sites and its tautomeric isomers of the Emodin in vacuum and in aqueous solution using polarizable continuum model (PCM), we conclude that the first deprotonation takes place at position 3 and the second at position 8. Considering a deprotonation at position 3, we calculated the standard first deprotonation free energy of Emodin in aqueous solution, by two different thermodynamic cycles and using an explicit model of the solvent, with Free Energy Perturbation theory in Monte Carlo simulation, ΔG_{aq} = 12.1 ± 1.4 kcal/mol, and for comparison with the polarizable continuum model (HF/3-31G(d)/PCM/UAHF), ΔG_{aq} = 11.6 ± 1.0 kcal/mol. Both solvent models gave theoretical results in very good agreement with the experimental estimated value of 10.9 ± 0.2 kcal/mol obtained from the acidity constant, pK_{a1} = 8.0 ± 0.1, using Eq. (9).

It is interesting to note (see Table 3) that the values obtained for the standard solvation free energy of the neutral and deprotonated species of Emodin in aqueous solution are significantly different, ΔG_{solv}(EMH) = −18.1 ± 0.7 (−11.6) kcal/mol and $\Delta G_{solv}(EM^-)$ = −55.0 ± 0.7 (−44.5) kcal/mol, for FEP-MC model (PCM) and this difference is caused mostly by the non-electrostatic terms. Therefore, we conclude that due to the cancelation of the non-electrostatic term of the deprotonation free energy, the calculation of this property is more accurate than the solvation free energy of the species involved in the deprotonation process.

Conflict of interest

The authors declare no conflict of interest.

Acknowledgements

Work partially supported by CNPq, CAPES, FAPESP, INCT-FCx, NAP-FCx(USP) and nBioNet (Brazil). Additionally, ARC acknowledges the fellowship from CNPq/CAPES, and MTL and KC research fellowships from CNPq.

Appendix A. Supplementary data

Supplementary data associated with this article can be found, in the online version, at http://dx.doi.org/10.1016/j.chemphys.2014.06.009.

References

[1] R.H. Thomson, Naturally Occurring Quinones, vol. 3, Chapman and Hall, London, New York, 1987.
[2] D.S. Alves, L. PérezFons, A. Estepa, V. Micol, Biochem. Pharmacol. 68 (2004) 549.
[3] H. Anke, I. Kolthoum, H. Laatsch, Biol. Act. Arch. Microbiol. 126 (1980) 231.
[4] T.L. Van, Acta Agrar. Silv. Ser. Agrar. 23 (1984) 235.
[5] W.H. Wang, J.G. Chung, Curr. Microbiol. 35 (1997) 262.
[6] D.L. Barnard, J.H. Huffman, J.L. Morris, S.G. Wood, B.G. Hughes, R.W. Sidwell, Antiviral Res. 17 (1992) 63.
[7] K. Kawai, T. Kato, H. Mori, J. Kitamura, Y. Nozawa, Toxicol. Lett. 20 (1984) 155.
[8] A. Kumar, S. Dhawan, B.B. Aggarwal, Oncogene 17 (1998) 913.
[9] Y.C. Kuo, H.C. Meng, W.J. Tsai, Inflammation Res. 50 (2001) 73.
[10] Y.C. Chen, S.C. Shen, W.R. Lee, E.L. Hsu, H.Y. Lin, C.H. Ko, S.W. Tseng, Biochem. Pharmacol. 64 (2002) 1713.
[11] G. Srinivas, R.J. Anto, P. Srinivas, S. Vidhyalakshmi, V.P. Senan, D. Karunagaran, Eur. J. Pharmacol. 473 (2003) 117.
[12] T.C. Chan, C.J. Chang, N.M. Koonchanok, R.L. Geahlen, Biochem. Biophys. Res. Commun. 193 (1993) 1152.
[13] L. Wang, L. Lin, B. Ye, J. Pharm. Biomed. Anal. 42 (2006) 625.
[14] S.T. Saito, G. Silva, C. Pungartnik, M. Brendel, J. Photochem. Photobiol. B 111 (2012) 59.
[15] G. Fabricíova, S. Sanchez-Cortes, J.V. Garcia-Ramos, P. Miskovsky, Biopolymers 74 (2004) 125.
[16] T. Pal, N.R. Jana, Analyst 118 (1993) 1337.
[17] S.C. Nguyen, B.K.V. Hansen, S.V. Hoffmann, J. Spanget-Larsen, Chem. Phys. 352 (2008) 167.
[18] G.H. Rochester, Acidity Functions, Academic Press, New York, 1971.
[19] C.R. Cantor, P.R. Schimmel, Biophysical Chemistry. Part III: The Behavior of Biological Macromolecules, W.H. Freeman and Co.,, New York, 1980.
[20] M. Uudsemaa, T. Kanger, M. Lopp, T. Tamm, Chem. Phys. Lett. 485 (2010) 83.
[21] J.B. Hansen, O. Hafliger, J. Pharmacol. Sci. 72 (1983) 429.
[22] S. Singh, D. Gupta, M.M. Tewari, P.C. Yadava, S.R. Tripathi, K.L. Yadava, Electrochim. Acta 39 (1985) 105.
[23] J. Pospichal, M. Deml, P. Bocek, J. Chromatogr. 390 (1987) 17.
[24] M. Roses, M.J. Bonet, E. Bosch, Anal. Chim. Acta 333 (1996) 241.
[25] S.-D. Kim, J.-K. Kim, Anal. Sci. Technol. 10 (1997) 256.
[26] D.L. Rabenstein, S.P. Hari, A. Kzerner, Anal. Chem. 69 (1997) 4310.
[27] J.B. Clistunoff, K.P. Johnston, J. Phys. Chem. B 102 (1998) 3993.
[28] J.Z. Yang, J. Liu, Thermochim. Acta 308 (1998) 171.
[29] A.G. Bezerra Jr., I.E. Borissevitch, A.S.L. Gomes, C.B. de Araújo, Opt. Lett. 25 (2000) 323.

[30] D. Wang, G. Yang, X. Song, Electrophoresis 22 (2001) 464.
[31] W.L. Jorgensen, J.M. Briggs, J. Gao, J. Am. Chem. Soc. 109 (1987) 6857.
[32] W.L. Jorgensen, J.M. Briggs, J. Am. Chem. 111 (1989) 4190.
[33] P. Beroza, D.R. Fredkin, M.Y. Okamura, G. Feher, Proc. Natl. Acad. Sci. USA 88 (1991) 5804.
[34] J.R. Pliego Jr., J.M. Riveros, J. Phys. Chem. B 104 (2000) 5155.
[35] B. Honing, K. Sharp, A.-S. Yang, J. Phys. Chem 97 (1993) 1101.
[36] H.W.T. van Vlijmen, M. Schaefer, M. Karplus, Funct. Bioinform. 33 (1998) 145.
[37] C.J. Cramer, D.G. Truhlar, J. Am. Chem. Soc. 113 (1991) 8305.
[38] C. Lim, D. Bashford, M. Karplus, J. Phys. Chem. 95 (1991) 5610.
[39] G. Schüürmann, M. Cossi, V. Barone, J. Tomasi, J. Phys. Chem. A 102 (1998) 6706.
[40] J.R. Pliego Jr., Chem. Phys. Lett. 367 (2003) 145.
[41] A. Klamt, F. Eckert, M. Diedenhofen, M.E. Beck, J. Phys. Chem. A 107 (2003) 9380.
[42] S. Zhang, J. Comp. Chem 33 (2012) 2469.
[43] C.P. Kelly, C.J. Cramer, D.G. Truhlar, J. Phys. Chem. B 110 (2006) 16066.
[44] D.M. Camaioni, C.A. Schwerdtfeger, J. Phys. Chem. A 109 (2005) 10795.
[45] R. Casanovas, J. Frau, J. Ortega-Castro, A. Salvà, J. Donosco, J. Mol. Struct. THEOCHEM 912 (2009) 5.
[46] A. Onufriev, D.A. Case, G.M. Ullmann, Biochemistry 40 (2001) 3413.
[47] H-.H. Perkampus, UV–Vis Spectroscopy and Its Applications, Springer-Verlag, Berlin, 1992.
[48] R.G. Parr, W. Yang, Density Functional Theory of Atoms and Molecules, Oxford Science Publications, Oxford, 1994.
[49] A.D. Becke, J. Chem. Phys. 98 (1993) 5648.
[50] Y. Imamura, T. Otsuka, H. Nakai, J. Comput. Chem. 28 (2007) 2067.
[51] D. Ditchfield, W.J. Hehre, J.A. Pople, J. Chem. Phys. 54 (1971) 724.
[52] D. Jacquemin, X. Assfeld, J. Preat, E.A. Perpete, Mol. Phys. 105 (2007) 325.
[53] Z.S. Marković, N.T. Manojlović, Monastsh. Chem. 140 (2009) 1311.
[54] J. Tirado-Rives, W.L. Jorgensen, J. Chem. Theory Comput. 4 (2008) (2008) 297.
[55] S. Miertus, E. Scrocco, J. Tomasi, Chem. Phys. 55 (1981) 117.
[56] J.E. Bartmess, J.A. Scott, R.T. McIver Jr., J. Am. Chem. Soc. 101 (1979) 6056.
[57] J.E. Bartmess, in: P.J. Linstrom, W.G. Mallard, NIST Chemistry WebBook, NIST Standard Reference Database Number 69, National Institute of Standards and Technology, Gaithersburg, March 2003, <http://webbook.nist.gov>.
[58] C. Møller, M.S. Plesset, Phys. Rev. 46 (1934) 618.
[59] R. Krishnan, J.A. Pople, Int. J. Quantum Chem. 14 (1978) 91.
[60] R.W. Zwanzig, J. Chem. Phys. 22 (1954) 1420.
[61] P.R. Schleyer (Ed.), Encyclopedia of Computational Chemistry, vol. 2, John Wiley & Sons, New York, 1998. D.A. Pearlman, B.G. Rao, p. 1036; W.L. Jorgensen, p. 1061; A.E. Mark, p. 1070.
[62] W.L. Jorgensen, C. Ravimohan, J. Chem. Phys. 83 (1985) 3050.
[63] W.L. Jorgensen, L.L. Thomas, J. Chem. Theory Comput. 4 (2008) 869.
[64] R.C. Guedes, K. Coutinho, B.J.C. Cabral, S. Canuto, J. Phys. Chem. B 107 (2003) 4304.
[65] H.C. Georg, K. Coutinho, S. Canuto, Chem. Phys. Lett. 413 (2005) 16.
[66] M.C.P. Lima, K. Coutinho, S. Canuto, W.R. Rocha, J. Phys. Chem. A 110 (2006) 7253.
[67] H. Pasalic, A.J.A. Aquino, D. Tunega, G. Haberhauer, M.H. Gerzabek, H.C. Georg, T.F. Moraes, K. Coutinho, S. Canuto, H. Lischka, J. Comput. Chem. 31 (2010) 2046.
[68] M.V.A. Damasceno, B.J.C. Cabral, K. Coutinho, Theor. Chem. Acc. 131 (2012) 1214.
[69] R.W. Taft, J.F. Wolf, J.L. Beauchamp, G. Scorrano, E.M. Arnett, J. Am. Chem. Soc. 100 (1978) 1240.
[70] A. Ben-Naim, Y.J. Marcus, J. Chem. Phys. 81 (1984) 2016.
[71] M.W. Palascak, G.C. Shields, J. Phys. Chem. A 108 (2004) 3692.
[72] M.D. Tissandier, K.A. Cowen, W.Y. Feng, E. Gundlach, M.J. Cohen, A.D. Earhart, J.V. Coe, J. Phys. Chem. A 102 (1998) 7787.
[73] M.P. Allen, D.J. Tildesley, Computer Simulation of Liquids, Clarendon, Oxford, 1987.
[74] K.J. de Almeida, K. Coutinho, W.B. de Almeida, W.R. Rocha, S. Canuto, Phys. Chem. Chem. Phys. 3 (2001) 1583.
[75] H.J.C. Berendsen, J.P.M. Postma, W.F. van Gunsteren, J. Hermans, in: B. Pullman (Ed.), Intermolecular Forces, Dordrecht, Reidel, 1981.
[76] W.L. Jorgensen, D.S. Maxwell, J. Tirado-Rives, J. Am. Chem. Soc. 118 (1996) 11225.
[77] W.L.C.M. Breneman, K.B. Wiberg, J. Comp. Chem. 11 (1990) 361.
[78] R.C. Barreto, K. Coutinho, H.C. Georg, S. Canuto, Phys. Chem. Chem. Phys. 11 (2009) 1388.
[79] V. Manzoni, M.L. Lyra, R.M. Gester, K. Coutinho, S. Canuto, Phys. Chem. Chem. Phys. 12 (2010) 14023.
[80] V. Manzoni, M.L. Lyra, K. Coutinho, S. Canuto, J. Chem. Phys. 135 (2011) 144103.
[81] W.L. Jorgensen, J.K. Buckner, S. Boudon, J. Tiradorives, J. Chem. Phys. 89 (1988) 3742.
[82] P. Cieplak, P.A. Kollman, J. Am. Chem. Soc. 110 (1988) 3734.
[83] P.F.B. Gonçalves, H. Stassen, J. Comput. Chem. 24 (2003) 1758.
[84] V. Barone, M. Cossi, J. Tomasi, J. Chem. Phys. 107 (1997) 3210.
[85] J. Ho, A. Klamt, M.L. Coote, J. Phys. Chem. A 114 (2010) 13442.
[86] T.N. Brown, N. Mora-Diez, J. Phys. Chem. B 110 (2006) 20546.
[87] T.N. Brown, N. Mora-Diez, J. Phys. Chem. B 110 (2006) 9270.
[88] M.J. Frisch, G.W. Trucks, H.B. Schlegel, G.E. Scuseria, M.A. Robb, J.R. Cheeseman, J.A. Montgomery Jr., T. Vreven, K.N. Kudin, J.C. Burant, J.M. Millam, S.S. Iyengar, J. Tomasi, V. Barone, B. Mennucci, M. Cossi, G. Scalmani, N. Rega, G.A. Petersson, H. Nakatsuji, M. Hada, M. Ehara, K. Toyota, R. Fukuda, J. Hasegawa, M. Ishida, T. Nakajima, Y. Honda, O. Kitao, H. Nakai, M. Klene, X. Li, J.E. Knox, H.P. Hratchian, J.B. Cross, V. Bakken, C. Adamo, J. Jaramillo, R. Gomperts, R.E. Stratmann, O. Yazyev, A.J. Austin, R. Cammi, C. Pomelli, J.W. Ochterski, P.Y. Ayala, K. Morokuma, G.A. Voth, P. Salvador, J.J. Dannenberg, V.G. Zakrzewski, S. Dapprich, A.D. Daniels, M.C. Strain, O. Farkas, D.K. Malick, A.D. Rabuck, K. Raghavachari, J.B. Foresman, J.V. Ortiz, Q. Cui, A.G. Baboul, S. Clifford, J. Cioslowski, B.B. Stefanov, G. Liu, A. Liashenko, P. Piskorz, I. Komaromi, R.L. Martin, D.J. Fox, T. Keith, M.A. Al-Laham, C.Y. Peng, A. Nanayakkara, M. Challacombe, P.M.W. Gill, B. Johnson, W. Chen, M.W. Wong, C. Gonzalez, J.A. Pople, Gaussian 03, Revision C.02, Gaussian Inc, Wallingford, CT, 2004.
[89] K. Coutinho, S. Canuto, DICE: A Monte Carlo Program for Liquid Simulation, University of São Paulo, São Paulo, 2003.
[90] C.R. Cantor, P.R. Schimmel, Biophysical Chemistry. Part II. Techniques for the Study of Biological Structure and Function, W.H. Freeman and Co., New York, 1980.
[91] A. Prakash, Z. Kristallogr. 113 (1965) 272.
[92] A. Prakash, Acta Cryst. 22 (1967) 439.